A study of the effects of side holes in indwelling needle for hemodialysis using computational fluid dynamis

Shimazaki Naoya [1], Nakane Noriaki [2], Yamauchi Shinobu [2], Motohashi Yuka [2], Sato Toshio [1, 2] and Agishi Tetsuzo [2]

[1] Graduate School of Engineering, Toin University of Yokohama
[2] Faculty of Biomedical Engineering, Toin University of Yokohama

（2017 年 3 月 18 日　受理）

Key Words : Hemodialysis, Indwelling needle, Computational fluid dynamics, Side hole, Blood flow rate

I. Introduction

Small-diameter indwelling needles are desirable to prevent deterioration in vascular access (VA) with frequent paracentesis and minimize puncture pain and maintain satisfactory VA while efficient dialysis is in progress in hemodialysis (HD). However, their use is reportedly associated with a widening divergence between set blood flow rate and actual blood flow rate as the former is increased. Hemodiafiltration (HDF) is a therapy combing HD and hemofiltration (HF), and it has been used for an increasing number of patients in recent years. Therapies involving higher settings for blood flow rate than the mean set blood flow rate in conventional HD (204.9 ± 36.4 ml/min) are also increasing. Boring side holes near the tip of the indwelling needle is one way to increase actual blood flow rate without changing the needle gauge or effective length. This measure is considered effective; however, increased flow resistance at blood removal has reportedly resulted from boring of side holes. We identified one factor as a possible cause of this phenomenon through measurement of the pressure distribution at the tip of the needle and visualizing blood flow at that location with particle image velocimetry (PIV) [1)]. We found that collision between blood flows from the hole at the needle tip and blood flows from the side holes of the indwelling needle obstruct blood removal from the hole at the needle tip. On the other hand, we have found few reports on optimum indwelling-needle tip shape with reference to the size, number and configuration of side holes for correction of the divergence between actual and set blood flow rates, or on factors that could reduce this divergence [2)]. Multiple prototypes could be created varying any needle-tip parameter that might affect blood removal properties; however, a clinical evaluation of their performance under uniform conditions in the same patients would

[1] Shimazaki Naoya, [2] Nakane Noriaki, [2] Yamauchi Shinobu, [2] Motohashi Yuka, [1, 2] Sato Toshio and [2] Agishi Tetsuzo
[1] Graduate School of Engineering, Toin University of Yokohama
[2] Faculty of Biomedical Engineering, Toin University of Yokohama. 1614 Kurogane-cho, Aoba-ku, Yokohama 225-8503, Japan

involve considerable expense and be very time consuming. Accordingly, we created an analysis model targeting indwelling needles with different configurations and investigated the theoretical effects of indwelling needle-tip side holes on blood removal properties with computational fluid dynamics (CFD).

II. Analysis and Experimental Methods

1. Analysis Model Creation and Analysis Conditions

The CFD software used in this study was ANSYS CFX (Cybernet Systems Co., Ltd.). The target of this analysis was a two-stage needle type of Medicut™ cannula with clamping tube (Covidien Japan Inc.) and 17G (1.5 mm) external diameter and 19G (1.3 mm) internal diameter. The cannula used for creation of the analysis model had an effective length of 30 mm (1088M17SCE, refer to ***Figure 1(a)***). Although this cannula has four side holes, the initial analysis model was based on a simple configuration without side holes in this research aimed at establishing a basic CFD technique for indwelling hemodialysis needles. The indwelling-needle analysis model created is shown in ***Figure 1(b)***. The needle base had a 4 mm internal diameter, a length of 59 mm, and a tip-to-base transfer distance of 4 mm. The analysis model simulated insertion of an indwelling needle into an artificial blood vessel (internal diameter:12 mm, length:150 mm) as shown in ***Figure 1(c)***. The angle of insertion into the artificial blood vessel was set at 25°, as the approximate angle recommended for an arteriovenous fistula (AVF) in guidelines on the creation and repair of VA in chronic HD patients. Needle insertion was against the direction of blood flow in the artificial blood vessel or arranged so as to leave the tip dwelling in the center of the artificial blood vessel. The analysis type was steady state, and the conditions for

(a) Actual indwelling needle

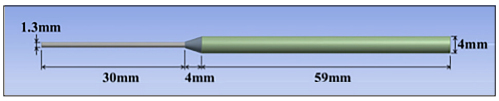

(b) Analysis model of indwelling needle

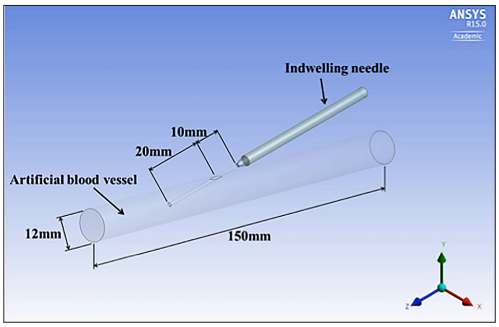

(c) Analysis model simulated insertion of an indwelling needle

Fig.1 Actual indwelling needle and corresponding analysis model

influx were set as follows: density (ρ) at the point of inflow from the artificial blood vessel was set at 997 kg/m^3; a flow rate of 700 ml/min for inflowing water (at a temperature of 25 °C) with a viscosity (μ) of 0.89 mPa·s; and a mean static pressure of 0 Pa as the setting for the flow at the outlet from the artificial blood vessel. Analysis results were obtained for water, though different results would have been obtained with the viscosity setting for blood (about 4 mPa·s); however, as stated above, we were initially prioritizing the establishment of a basic analysis technique, and we decided to use water in this research for the purpose of simplifying the analysis. The setting for wall surface condition was set at "NoSlipWall" to match the wall surface velocity with the rate of flow.

2. Measurements of Blood Removal Pressure for Setting Analysis Conditions

CFD analysis also necessitated measurement of blood removal pressure at the needle base end

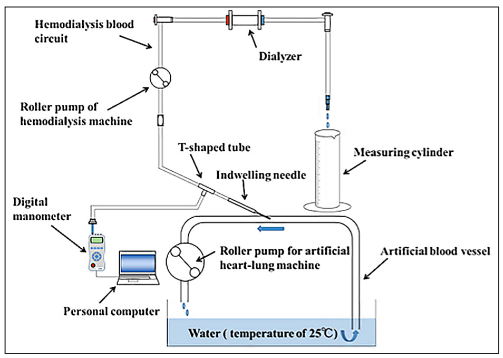

Fig. 2 Measurements of blood removal pressure and actual blood flow rate

as shown in ***Figure 1(c)***, in addition to the setting of analysis conditions described in the previous section. Accordingly, we carried out an experiment for this blood pressure measurement. To obtain an indwelling needle with the same configuration as the analysis model (effective length 30 mm; no side holes), a similarly configured cannula (1088M17CE) with the same external diameter but an effective length of 50 mm was used. The 1088M17CE cannula was cut 20 mm from its tip to obtain an indwelling needle with the same effective length as that in the analysis model (30 mm) and without side holes. As shown in ***Figure 2***, this needle tip was positioned to dwell in the center of a vinyl chloride artificial blood vessel. The internal diameter of the artificial blood vessel was 12 mm, and the angle of injection was 25°. Hemodialysis blood circuit (NV-Y030P, Nikkiso Co., Ltd.) was filled with water, and the arterial line of the blood circuit was attached to the connector of the indwelling needle. A dialyzer (BK-1.3U, Toray Industries, Inc.) was connected between arterial and venous line of blood circuit. The blood flow at removal was between 50 ml/min and 300 ml/min on a hemodialysis machine (DCS-73, Nikkiso Co., Ltd.) and was set at 50 ml/min intervals. A roller pump (Multiflow, Staccato, Co., Ltd.) for an artificial heart-lung machine was used to circulate water (at a temperature of 25 °C) in a counter-current to the indwelling needle at a flow rate of 700 ml/min in the artificial blood vessel. A T-shaped tube was attached between the needle and the roller pump of the hemodialysis machine, and a digital manometer (EM-160W, -749.9hPa to +1499.9hPa, Hodoka Corp.) was connected to the T-shaped tube to measure blood removal pressure. This arrangement was used to measure blood removal pressure for each set blood flow rate. Before initiating the water circulation in the artificial blood vessel and blood removal from the indwelling needle, the digital manometer was calibrated (set to zero) in lentic state. Blood removal pressure at the needle base end was measured at 0.5-second intervals every 30 seconds for each set blood flow rate. Blood removal pressure was measured repeatedly, five times, for each set blood flow rate, and mean blood removal pressure was calculated. The obtained blood removal pressure shown in ***Figure 1(c)*** was set as the blood removal pressure for the needle base end.

We set out to demonstrate the suitability of the CFD analysis by comparing the actual blood flow rates with those obtained in the CFD analysis, for each set blood flow rate in this study. At the time of measuring blood removal pressure for each set blood flow rate, the volume of blood outflow at the end of the venous line was collected for a 1-minute period with a 500-ml measuring cylinder to determine the actual blood flow rate. Actual blood flow rate measurements were performed repeatedly (10 times), and mean values were calculated for each set blood flow rate.

III. Analysis and Experimental Results

1. Blood Removal Pressure of Indwelling Needle

Blood removal pressure was measured to determine its setting at the indwelling-needle base end for the analysis model (***Fig. 1(c)***). The measurement results are shown in ***Figure 3***. An exam-

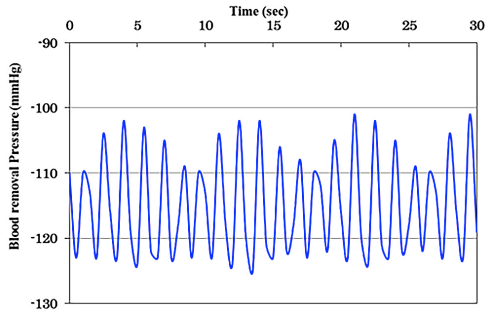

(a) Change with time of blood removal pressure (blood flow rate: 200 ml/min)

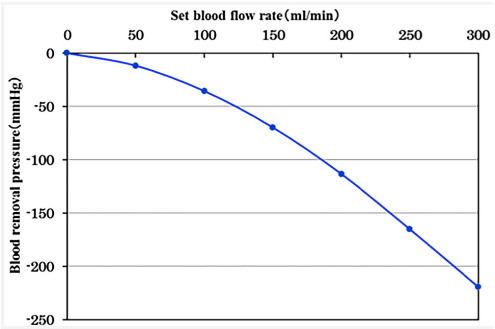

(b) Blood removal pressure for each set blood flow rate

Fig.3 Results of blood removal pressure measurement

ple of the serial blood removal pressure measurements made with the digital manometer is shown in ***Figure 3(a)***; these measurements were performed in 30-second installments with set blood flow rate at 200 ml/min. An occluded tubing was opened when it was separated from the roller of the roller pump. There was a slight fall in pressure at this time, which resulted in periodic fluctuation in blood removal pressure between −102 mmHg and −125 mmHg. In this case, the periodic fluctuation occurred approximately every 1.5-seconds, a half rotation cycle for the pump. In this study, blood removal pressure was defined as the mean value for a 30-second measurement period, and the standard deviation did not exceed approximately 3% for any set blood flow rate, demonstrating high reproducibility for the results of this study.

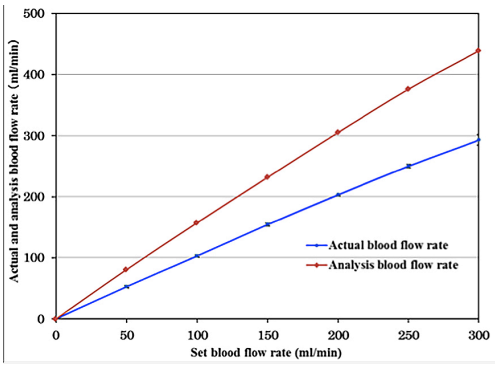

Fig.4 Comparison between actual and analysis blood flow rate

2. CFD Analysis-derived Blood Flow Rates and Actual Blood Flow Rates

The blood removal pressure for the needle base end in the analysis model (***Fig. 1(c)***) was set from the results of blood removal pressure measurements at indwelling needle base end. The blood flow rates obtained from this no-side-hole analysis model in the CFD analysis (Q') are shown against the actual blood flow rates (Q_0) in ***Figure 4***. When Q was 250 mm/min or below, the difference with Q_0 was nearly zero. However, when Q was 300 ml/min, Q_0 was 292.9 ml/min, and ΔQ calculated as $\Delta Q = \frac{Q_0 - Q}{Q}$ was −2.4 %. As Q increased, Q_0 decreased, and the divergence between Q and Q_0 became greater.

Contrastingly, viewing Q' against Q_0 gave the results stated below. Q' was a significantry large value than Q_0. When Q_0 was 50 ml/min, Q' was 80.6 ml/min, and ΔQ' calculated as $\Delta Q' = \frac{Q - Q_0}{Q_0}$ was exceedingly large, at +61.2 %. The smallest difference between Q' and Q_0 was noted when Q was 300 ml/min, with Q' at 436.8 ml/min and ΔQ at +45.6 %.

IV. Discussion

The analysis-derived blood flow rate Q' was more than several tens of percent greater than the actual blood flow rate Q_0, irrespective of the setting for blood removal pressure (determined from results for blood removal pressure at the indwelling needle base end) in the CFD analysis, as described in Section III.2.

The sources of error in CFD analysis are considered to be related to the boundary conditions. Real space cannot be entirely reproduced in analysis; therefore, the domains that can be set in the analytical space are finite, and boundary conditions need to be set for the boundary surfaces between the analytical space and the space external to it. Blood removal pressure at the needle base end needed to be set in the present study (***Fig. 1(c)***), and blood removal pressure had a direct effect on the determination of Q'; therefore, blood removal pressure at an actual needle base end was measured against that in the analysis model, and the obtained results were set as boundary conditions. However, Q' was still more than several tens of percent greater than Q_0. This was caused as the effect of pressure loss not accounted for in the analysis model.

In an instance with the set blood flow rate Q at 200 ml/min, we set out to adjust Q' to Q_0, as follows. We assigned a value of $P_0 = -107.2$ mmHg (determined as described in Section II.2 for the removal pressure setting) to the removal pressure for the needle base end in analysis, and determined Q' while gradually reducing this removal pressure. Q' was adjusted to Q_0 when the analysis blood removal pressure (P') was −55.5 mmHg. Specifically, a pressure loss (ΔP) of 58 mmHg, which was not accounted for in the CFD analysis, emerged. We consider this pressure loss was produced by the blood circuit, dialyzer, or roller pump. The liquid friction resulting from the viscosity of the water flowing through the blood circuit produces pressure loss. Another pressure loss is produced by the occlusion of the pump tube of the roller pump. These pressure losses need to be accounted for in the analysis model. Fluid flowing inside the hollow fibers of the dialyzer can be regarded as infiltration flow running through the porous media due to the pressure gradient, and the resultant pressure loss must also be considered. Accordingly, we introduced the isotropic fluid resistance model, developed as an ANSYS CFX sub-domain, into this study.

Fluid resistance (S [Pa/m]) is determined by the equation shown below.

$$S = \frac{\mu}{K_{perm}} \cdot v + K_{loss} \cdot \frac{\rho}{2} \cdot v^2 \qquad (1)$$

In this equation, ρ [kg/m^3] represents fluid density, μ [Pa·s] represents the viscosity coefficient, and v [m/s] represents cross-sectional mean velocity. The first term of Equation (1) expresses the pressure loss obtained from infiltration flow with Darcy's law, and K_{perm} [m^2] represents permeability. The second term of Equation (1) expresses the pressure loss produced by the liquid friction resulting from viscosity with the Darcy-Weisbach equation, and K_{loss} [1/m] represents the pressure loss coefficient. At this point, length in the introduced fluid resistance model was set as L [m], and corrected pressure loss (ΔP [Pa]; correction required for value from Equation (1)) was calculated with the equation below.

$$\Delta P = \frac{\mu \cdot L}{K_{perm}} \cdot v + K_{loss} \cdot \frac{\rho \cdot L}{2} \cdot v^2 \qquad (2)$$

ΔP values had to be accounted for to produce convergence between Q' and Q_0 for each Q value, and they were calculated. The cross-sectional mean velocity v was calculated from the actual flow rate Q_0 for each Q value. Results are expressed by plotting v on the horizontal axis and ΔP along the vertical axis, as shown in ***Figure 5***. Regarding the intercept of the curve shown in Figure 5 as the origin, an approximate curve was obtained

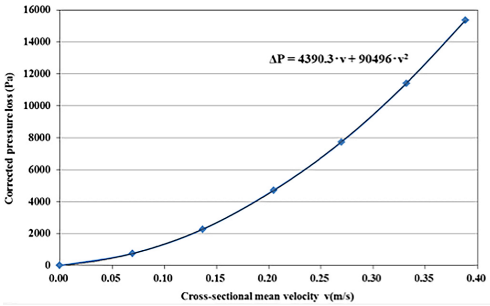

Fig.5 Relationship between cross-sectional mean velocity and corrected pressure loss

with second-order polynomial approximation, which produced the equation stated below.

$$\Delta P = 4390.3 \cdot v + 90496 \cdot v^2 \qquad (3)$$

Regarding length L in the fluid resistance model as 10 mm, permeability and pressure loss coefficients are obtained by comparing the v and v^2 from Equations (2) and (3) as follows : $K_{perm} = 1.060 \times 10^{-9}$ [m^2], $K_{loss} = 1.515 \times 10^4$ [1/m].

We introduced the fluid resistance model (with L = 10 mm) for the indwelling needle base, and set K_{perm} and K_{loss} for this model. We set the blood removal pressure obtained for each Q value in the experiment described in Section II.2. for the fluid-resistant end. We then carried out CFD analysis again to obtain the Q' values. Prior to the introduction of the fluid resistance model, Q' ranged from +45.6 % to +61.2 % against Q_0 for Q values between 50 ml/min and 300 ml/min. However, the corresponding range after model introduction was −0.3 % to +0.92 %, and near-exact calculation of Q' became possible.

V. Conclusion

We created an analysis model targeting indwelling needles with different configurations and investigated the theoretical effects of indwelling needle-tip side holes on blood removal properties with computational fluid dynamics (CFD). By introducing the fluid resistance model, Q' ranged from -0.3 % to +0.92 % against Q_0 for Q values, and near-exact calculation of Q' became possible.

[References]

1) S. Yamauchi *et al*., "Effects of side holes on blood removal characteristics based on measurement of the pressure distribution inside dialysis puncture needles", *Toin Research Bulletin* No.34, pp.91–96, *2016*.

2) Mehta HK *et al.*, "Correction of discrepancy between prescribed and actual blood flow rates in chronic hemodialysis patients with use of large gauge needles", *Am J Kidney Dis*. 2002 jun; 39(6):1231–5.